New Results on Terahertz Detection by Carbon Nanotubes

Enrique Carrion, Martin Muthee, Jason Donovan, Richard Zannoni, John Nicholson, Eric Polizzi and K. Sigfrid Yngvesson, *Life Fellow, IEEE*

Abstract—Since our first report on terahertz detection by bundles of single wall carbon nanotubes (SWCNTs) at the ISSTT2008, we have fabricated a large number of additional antenna-coupled SWCNT devices that all show terahertz detection. The maximum voltage responsivity (S_V) is about 25 V/W (intrinsic value 50 V/W) at 4.2 K, and S_V decreases slowly with temperature up to about 100 K. In this paper we further explore different fabrication procedures and the bolometric detection process. We also demonstrate diode type detection at terahertz frequencies in SWCNTs for the first time. We present results of circuit simulations and *ab initio* simulations of the electronic properties of SWCNTs.

***Index Terms*—Nanotechnology, carbon nanotubes, detectors, terahertz.**

I. INTRODUCTION

Our first paper at the **ISSTT** symposia on the topic of Terahertz detection in carbon nanotubes (CNTs) was presented at **ISSTT2005** [1]. We also discussed this topic in ref. [2]. At the **ISSTT2006** we presented results of microwave (MW) direct and heterodyne detection in *metallic* single wall carbon nanotubes (m-SWCNTs) [3],[4]. Very recently, the Yale group of D. Prober reported MW detection in m-SWCNTs [5], as well as a tentative terahertz detection [6]. Other groups have also demonstrated MW detection in SWNTs, primarily in *semiconducting* tubes (s-SWCNTs) [7]-[11]. McEuen et al. [12] used THz time-domain techniques for detection in a quasi-metallic (qm) SWCNT FET type device. The effective frequencies in that experiment were in the range of a few hundred GHz. Photoconductive detection in SWCNTs is very weak [13], but Itkis et al. [13] have developed a sensitive *bolometric* Near Infrared detector based on a Carbon Nanotube (CNT) film. Our group reported the first terahertz detection in bundles containing m-SWCNTs [14], up to 2.5 THz. The SWCNT bundles were coupled to log-periodic antennas in much the same manner as is used to couple NbN HEBs. At **ISSTT2008** we gave further results for this detector [15], as well as accurate characterization of the devices at microwave frequencies (up to 20 GHz). We also interpreted the experimental terahertz detection based on a general bolometric model. In the present paper, we further explore this bolometric model to interpret measured data for a large number of additional devices, which have been fabricated employing new methods. We also report a diode type of detection mode that was previously only seen at MW frequencies, but that we have now demonstrated in two devices up to frequencies as high as 1.6 THz.

CNTs are a promising medium for future terahertz detectors based on some general features based on their small diameters (1-2 nm) which lead to very low heat capacity and low capacitance. They can also have near ideal transport properties (ballistic transport) for both electrons and phonons. Detection in m-SWNTs can occur due to two basic mechanisms: (1) *a diode type* mechanism, as was proposed for terahertz in [7] and demonstrated at microwaves in [4]-[6]; (2) a *bolometer type* mode, similar to that in HEBs and other terahertz bolometers [5],[6],[14]-[16]. Both modes will be discussed below.

II. CHARACTERISTICS OF CARBON NANOTUBES

It is important to first review some general characteristics of CNTs. CNTs can be grown using several different methods, the main ones being laser ablation of carbon targets and chemical vapor deposition (CVD). Depending on the specific conditions during growth either multi-wall CNTs (MWCNTs) or SWCNTs may be formed. Although any type of CNT might be considered for terahertz detection we have concentrated on SWCNTs. SWCNTs can be conceptually viewed as a sheet of hexagonally arranged carbon atoms (called grapheme) that has been rolled up into a tube. This process can "work" for a large number of different wrapping angles, resulting in CNTs that differ in terms of their chirality. It was quickly realized that SWCNTs of different chirality can either be metallic (no bandgap at the Fermi level) or semiconducting (with bandgaps of from a few tenths of eV to about 1 eV, inversely proportional to the tube diameter). In a typical process about one third of the tubes are metallic, two thirds semiconducting. They can be distinguished experimentally since the resistance of the s-SWCNTs can be varied by application of a gate voltage to a back-contact substrate gate (or a top gate). The m-SWNTs then show constant resistance independent of the gate voltage. There are also cases in which tubes are nominally

Manuscript received 20 April 2009. This work was supported in part by the U.S. National Science Foundation under Grants ECS-0508436 and ECS-0725613.

All authors are with the Department of Electrical and Computer Engineering, University of Massachusetts/Amherst, Amherst, MA 01003, USA (corresponding author can be reached at phone: 413-545-0771; fax: 413-545-4611; yngvesson@ecs.umass.edu).

metallic, but in which perturbations create a small bandgap, typically 10 meV. Small bandgap tubes (also called quasi-metallic tubes, qm-SWNTs) and actual m-SWCNTs are often difficult to distinguish experimentally. In this paper we will characterize both as m-SWCNTs, unless otherwise noted.

As grown SWCNTs naturally form bundles of tubes due to the strong interaction between individual tubes. Many different surfactants have been used to separate the tubes. However, it has been found that the surfactants that remain on the tubes often cause the contacts to be unreliable and to have high resistance. In our work so far, we have usually employed bundles of tubes, although our initial MW detection [3],[4] was performed on single tubes. For both bundles and single tubes, special methods must be used to achieve low contact resistance. Tubes deposited on top of the contact metal usually result in contact resistances in the hundreds of kΩ for a single tube, even after a typical annealing procedure of two hours at 200°C-300°C. Lower contact resistance requires that the contact metal be deposited *on top of* the CNT, or surrounding it completely. The best known contact metal is palladium. In this case the total contact resistance can approach the quantum resistance of $h/4e^2$ = 6.45 kΩ. Although it may appear that SWCNTs with high contact resistance would not have good potential as terahertz detectors, we have discovered that this is not necessarily true, as we described at the last ISSTT [15]. Specifically, our MW probe measurements showed that the contacts include a large capacitance (1-20 fF) in parallel with the contact resistance that effectively shunts the contact resistance at terahertz frequencies. These measurements were performed on a different Coplanar Waveguide structure, not the same as the antennas we employed at THz. It is therefore likely that the range of contact capacitance for our THz devices is different, as will be discussed further below. All of the above types of tubes show nonlinear IV-characteristics that may potentially be considered for terahertz detection. We show typical examples below. The first example is a single m-SWNT with high contact resistance from our early work [3],[4].

This IV-curve has a nonlinearity at low bias voltage that is known as a "Zero-Bias Anomaly (ZBA)" [17]. The ZBA is interpreted as being due to tunneling through a barrier at the contacts. Higher bias voltage *increases* the tunneling current in this case. The resistance *increases* at lower temperatures as fewer electrons are able to tunnel. Bundles of tubes, as used in all of our more recent experiments show a very similar nonlinearity [15]. In this case we interpret the conductance of the bundle as being almost entirely due to the metallic tubes, since the s-SWCNTs are know to generally have much higher resistance.

An example of an IV-curve for a device with low contact resistance is given in Figure 2 below. This device was fabricated with Ti+Pd contacts below the CNTs, and Pd+Au above.

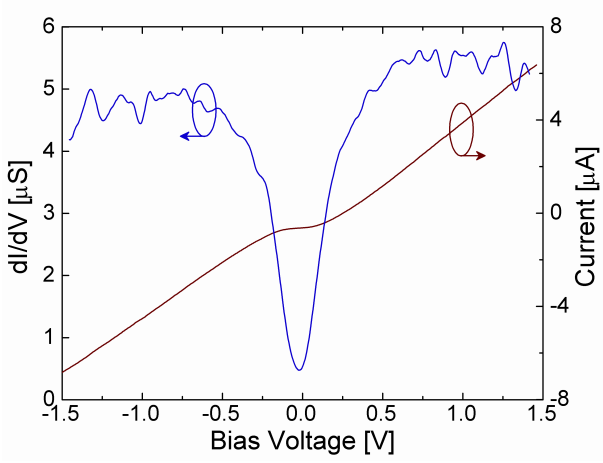

Figure 1. Typical IV-curve for a single m-SWCNT with high resistance contacts, from [4].

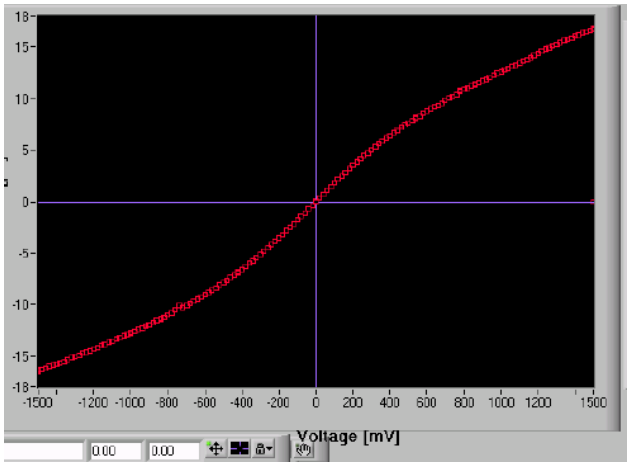

Figure 2. IV-curve for device with low contact resistance.

Clearly, the curvature in this case is in the opposite direction to that in Figure 1. The resistance is known to increase for bias voltages above 0.15 V due to optical phonon emission [17]. The resistance *decreases* at lower temperatures where fewer phonons exist that can scatter the electrons, as measured for example in [5]. The IV-curves shown in Figures 1 and 2 are for tubes supported by the silicon substrate. *Bundles of tubes* with low contact resistance have IV-curves with the same curvature [18].

Metallic SWCNTs can also be fabricated such that they are suspended across a trench that has been etched between the contacts. In this case the IV-curve at high voltages actually develops a negative slope (a negative differential resistance, NDR) due to very strong heating of the tubes [19].

In this work, we used nonconductive sapphire, silicon on sapphire (SOS) or high-resistivity silicon substrates. The choice of these substrates was crucial since for example highly doped silicon substrates show very strong absorption of THz. The sapphire, SOS and high resistivity silicon substrates have similar dielectric permittivity and are expected to all work well with the silicon lens quasi-optical coupling scheme we

employ (see Sec. IV.A). So far we have found no significant differences between these substrates.

We fabricated the CNT devices by the dielectrophoresis (DEP) method [20]. Typically, we apply a 5 - 50 MHz voltage of about 8V peak to Au contacts made by UV photolithography, such as those shown in Figure 3. We employed two types of log-periodic toothed antennas. LPA1 has about an 8 μm gap, as shown in Figure 3 (left). LPA 1 has an estimated upper frequency limit of 1.5 THz. We also fabricated LPAs with a smaller gap, about 1 μm (LPA2), as well as smaller teeth, see Figure 3 (right). LPA 2 has an estimated upper frequency limit of 3.5 THz. The LPA2 design is identical to one we used in our earlier NbN HEB work [21].

A drop of a suspension of CNTs in isopropyl alcohol [22] was applied to these structures. In the devices presented here we did not use surfactants, and consequently expect the tubes to be present in bundles. The CNTs will drift to the narrow gap in the contacts and attach to these, when the RF voltage is applied across the contacts. We monitor the DC resistance simultaneously through a bias tee. The DEP process is halted when the dc resistance is sufficiently low. All devices were annealed in air at 200 ^{o}C for two hours which decreased the contact resistance. The result is a small number of CNTs bundles contacted in parallel across the gap. The lower resistance of these devices, compared with the typical single SWCNTs, from 7 to 80 kΩ, facilitates matching of terahertz radiation to the CNTs. The IV-curves of all devices display the same "ZBA" that we had previously observed for the single m-SWNTs. The nonlinearity of the IV-curves is more pronounced the lower the temperature is, see Figure 4. We conclude that the IV-curves are due to a number of parallel metallic tubes in the bundles. Although DEP tends to primarily align m-SWCNTs, the bundles undoubtedly contain s-SWCNTs but these do not have any effect on the DC resistance.

In our initial device fabrication using antennas LPA1 and LPA2 we found by SEM and AFM imaging that the CNTs did not only attach to the smallest gap. Examples are shown in Figure 5. By using lower concentrated solutions and by centrifuging the solution to separate out impurities we obtained improved results.

We were also concerned about minimizing the thermal conductance, as discussed in Sec. IV.C. and therefore fabricated antennas that had an etched trench in the gap. These devices were fabricated on an oxidized high-resistivity silicon substrate with antennas of type LPA2 employed as etching mask for RIE. We term LPA2 antennas with a trench "LPA3".

Figure 3. Log-periodic antenna LPA1 (left) and LPA2 (right).

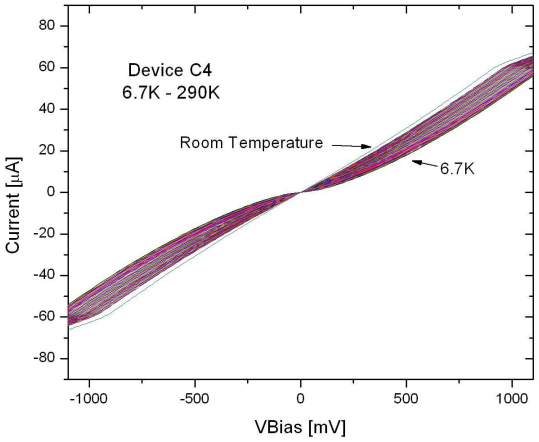

Figure 4. IV-curves as a function of temperature. Note that the non-linearity increases with decreasing temperature.

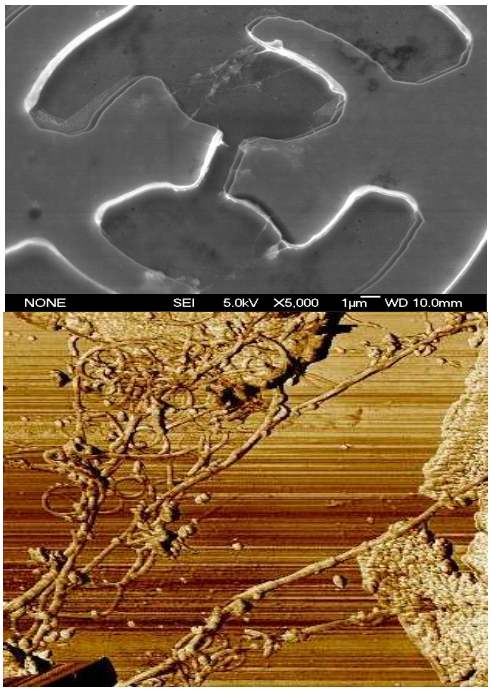

Figure 5. SEM and AFM pictures showing CNT bundles attached to some of the outer teeth of the antenna.

To further improve the probability of placing the tubes in the antenna gap we also applied photo resist and etched a small window that covered the antenna gap, see Figure 6. The DEP was then performed on the devices in this form. After the photoresist was dissolved, the CNTs remained in the gap (see Figure 7). It is not easy to ascertain from such pictures whether the tubes are actually suspended, and further SEM/AFM will be performed to answer this question.

III. DETECTION MODELS

Before presenting our experimental results we want to review the different models for the THz detection process in SWCNTs that we will consider.

A. The "diode" model

The voltage responsivity (S_V) and the current responsivity (S_I) are defined as

$$S_V = \Delta V/P_{THz} = S_I * R \qquad (1)$$

From standard microwave diode detector theory it is known [23] that

$$S_I = (1/4)*(d^2I/dV^2)*V^2_{THz}/P_{THz} \qquad (2)$$

Here, ΔV is the detected change in dc voltage, V_{THz} is the *peak* THz voltage and P_{THz} is the available THz power from the source.

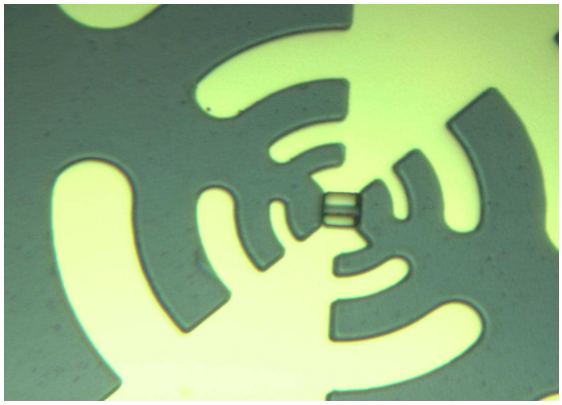

Figure 6. Optical photograph of an LPA3 antenna with an etched window for improved CNT placement in the antenna gap.

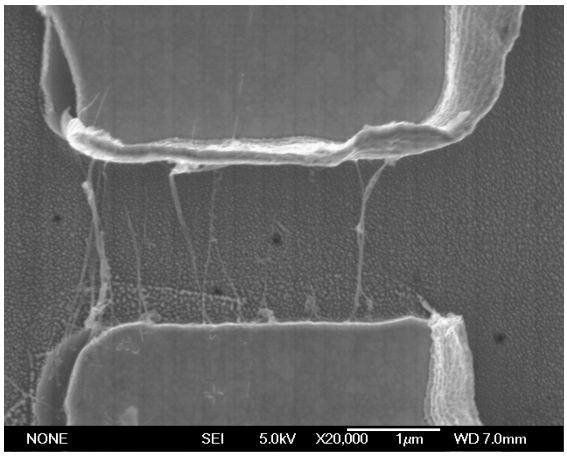

Figure 7. SEM picture of the gap region of an LPA3 antenna with several CNT bundles across the gap.

The only difference between the m-SWNT detector and MW diodes is that the m-SWNT IV-curve is symmetric. In [3],[4],[15] we showed that the MW voltage responsivity varies with bias voltage as $R*(d^2I/dV^2)$, which was obtained from the measured IV-curves. The agreement with Equations (1) and (2) was excellent. Note that for the devices in [3],[4],[15] the contact resistance was much larger than the actual CNT resistance, i.e. the nonlinearity of the IV curve could be ascribed to the contact resistance. Diode model fits could also be obtained for devices with low contact resistance, with IV-curves such as that in Figure 2, and by devices fabricated by the Yale group in [5,6]. In this case the nonlinearity is due to the CNT resistance, not the contact resistance. The Yale group reports a voltage responsivity of close to 400,000 V/W, measured at 77K and a frequency of 17 MHz [6]. **This makes it clear that the potential performance of SWCNTs as terahertz detectors is excellent.**

B. Bolometer Models

In bolometric detection the device changes its resistance in response to absorption of RF radiation. As the bolometer is heated by the terahertz power and biased by the dc current I_0, its temperature increases from T_0 to $T_0 + \Delta T$. If we define the factor $b = (1/R)*dR/dT$, then the voltage responsivity of the bolometer will be (neglecting electro-thermal feedback which is only important when the responsivity is very high) [24]:

$$S_V = \Delta V/P_{THz} = \frac{I_0 * R * b}{[G_{th} + i\omega C_h]}(V/W) \qquad (3)$$

A block-diagram of a bolometer is shown in Figure 8. The thermal time-constant of the bolometer is determined by $\tau_{th} = C_h/G_{th}$. In MW measurements on single qm-SWCNTs the Yale group showed that the response was typically consistent with a bolometer process due to heating of the SWCNTs [5],[6] (the contacts had very low resistance). This group measured dR/dT and showed that the change in resistance with temperature could be directly related to the DC heating as the bias voltage was increased. In this case DC heating and MW heating have equivalent effects on the resistance as in the "*standard model*" of HEBs [25]. RF absorption causes an *increased* resistance for the single tube case [5],[6].

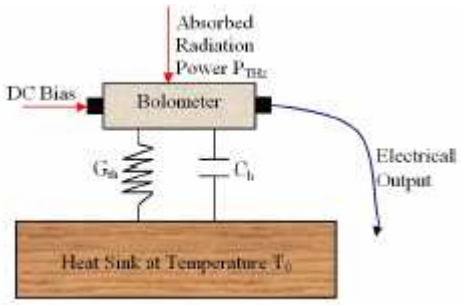

Figure 8. A bolometer model

We mention the above data in order to compare with our own THz detection results. A different type of bolometer model will be used below to interpret these: The *two-step bolometer model*. In this model, the THz radiation is absorbed in the m-SWCNTs which are therefore heated. The heated electrons in the CNTs then create an increased dc tunneling current through the contacts. The result of the THz absorption is thus a *decreased* resistance, equivalent to what happens when the entire device is heated. The net result is that equation (3) can still be used, by inserting measured values of dR/dT. One difference to the standard model case is that dR/dT depends on the bias voltage even under constant temperature conditions.

IV. TERAHERTZ MEASUREMENTS AND MODEL ANALYSIS

A. THz Measurement Setup

For the terahertz measurements, a device chip with dimensions 6x6 mm^2 was inserted in a fixture available from our earlier work with NbN HEB receivers [21]. The fixture allowed quasi-optical coupling to terahertz radiation, as well as bias input and detector output through a coaxial cable. Gold bond wires were used to connect to the contact pads of LPA1, while indium wires could be employed for LPA2, which has considerably larger contact pads. The fixture was then mounted in a liquid helium dewar. A 4 mm diameter ellipsoidal silicon lens was attached to the substrate for quasi-optical coupling to the antenna as shown in Fig. 9.

A 100 kΩ resistor is connected in series with the carbon nanotube, and the Keithley Source Meter is connected directly to the resistor (Figure 10). The dc voltage across the two terminals of the carbon nanotubes is sensed at the V_{sense} port. The Source Meter also measures the current through the carbon nanotubes. A change in the device current gives rise to a voltage drop across the 100 kΩ resistor that is measured with a lock-in amplifier (EG&G 7260), which has an input impedance of 1 MΩ, through two 200 kΩ resistors. A 1 kHz signal from a function generator was employed as reference for the lock-in amplifier.

Terahertz radiation was introduced through the dewar window and the silicon lens from a CO_2-laser (Coherent/DEOS GEM-50) pumped terahertz gas laser that had a typical output power of 2-5 mW (Figure 11). The power was measured with a Scientech (Astral AA30) power meter. The laser was modulated from the same 1 kHz function generator by inserting an acousto-optic modulator (IntraAction AGM-406B21) after the CO_2 pump laser, as indicated in Figure 10.

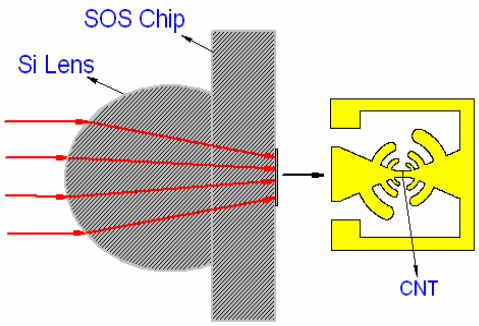

Figure 9. The quasi-optical coupling configuration.

B. Overview of Terahertz Measurement Results

Using the configuration described in section IV.A we have demonstrated THz detection in CNT bundles at several different frequencies (from 0.694 THz to 2.54 THz). We have measured the response for 18 devices of quite different resistances; see Table I for some examples. The resistance values given are for 300 K and low bias voltage.

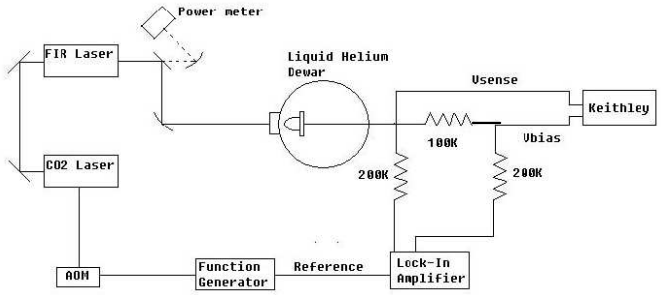

Figure 10. THz measurement setup.

Figure 11. Photograph of the terahertz gas laser source.

TABLE I.

Device	Resistance (kΩ)	Antenna	# Active m-SWNTs
B2	20	LPA1	50
C1	7	LPA2	30
C4	16	LPA2	15
1C4	80	LPA3	20
2D1	70	LPA3	20
3C3	50	LPA3	10*
4B2	40	LPA3	80*
4A2	22	LPA3	7*
4A3	48	LPA3	40*
2B1	16	LPA3	20*

*Estimates based on SEM imaging.

A summary of the voltage responsivity for selected terahertz detections is given in Figure 12. The terahertz power was measured outside the window of the dewar, and the response was linear in power. There is a roughly 3 to 4 dB optical loss between the dewar window and the antenna terminals, which was not corrected for. It is clear that there is a general type of detection process that works for a wide range of terahertz frequencies. There appears to be a pattern of decreasing responsivity from 0.694 THz to 1.63 THz, except for Device B2 that increased its responsivity at 2.54 THz.

Some devices show no or only very weak detection at 300 K, but Device 1μmB2 is an exception to this rule (not shown in Figure 13 or Table I). Up to about 100 K, the responsivity depends only weakly on temperature, typically decreasing only a factor of two or less from 4.2 K to about 25 K. The largest responsivity measured is about 25 V/W, which would

correspond to an intrinsic responsivity (correcting for optical losses) of over 50 V/W. We first discuss the results which can be interpreted using the bolometric model.

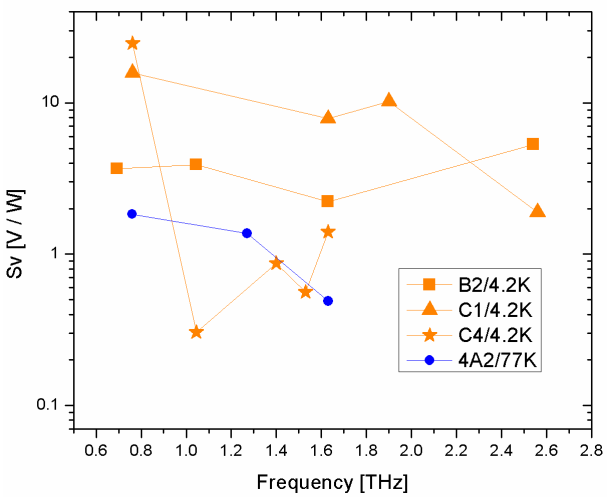

Figure 12. Summary of measured THz responsivity versus frequency.

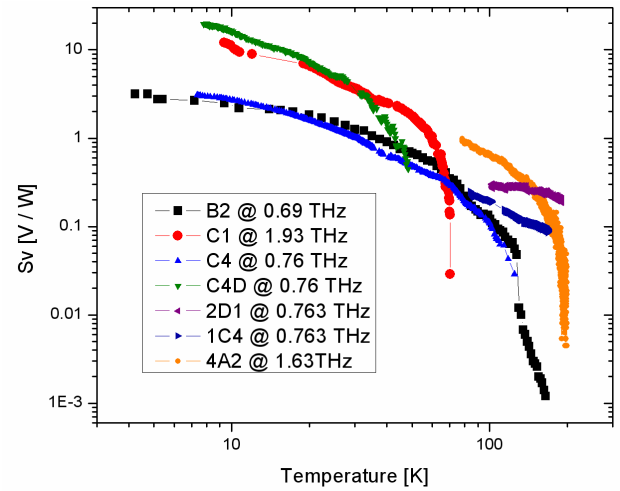

Figure 13. Summary of measured THz responsivity versus temperature.

C. Devices That Conform to The Bolometric Model

The criterion for whether a device conformed to the bolometer model was whether the responsivity followed Eq. (3) as the voltage bias was varied. We first measured R(T) versus voltage at several different temperatures, see Figure 14, and then calculated the factor b = 1/R*(dR/dT), Figure 15. Using this data we then varied the unknown factor G_{th} to obtain a best fit to Eq. (3), see Figures 16 and 17. Good fits were obtained for all devices (excepting two devices discussed in the next section), and at all frequencies at which they were measured. On the other hand, it was not possible to obtain a fit to Equations (1) and (2) for the diode mode. The voltage for which S_V peaks is about 60 mV at 5 K and 700 mV at 77 K. Note that the device temperature is not expected to change as the bias voltage is changed, since there is negligible DC heating of the CNTs. We thus expect that a single value of G_{th} should be valid for the entire curve. We have plotted G_{th} as a function of temperature in Figure 18, and compared with G_{th} for a single tube, as measured in [5,6]. The temperature dependence for single tubes and bundles appears to be quite similar at the lowest temperatures, but somewhat faster for the bundles above 60 K.

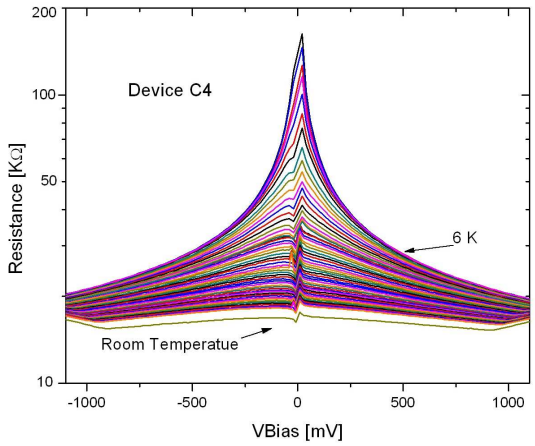

Figure 14. Measured resistance of device C4 for several different temperatures from 300 K to 5 K, versus bias voltage.

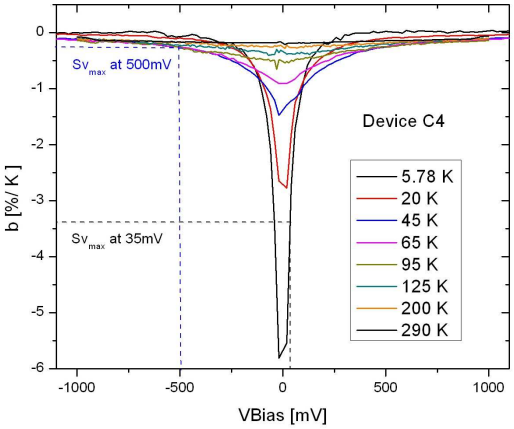

Figure 15. Plots of the factor 'b' in Eq. (3) for device C4 versus bias voltage for several different temperatures.

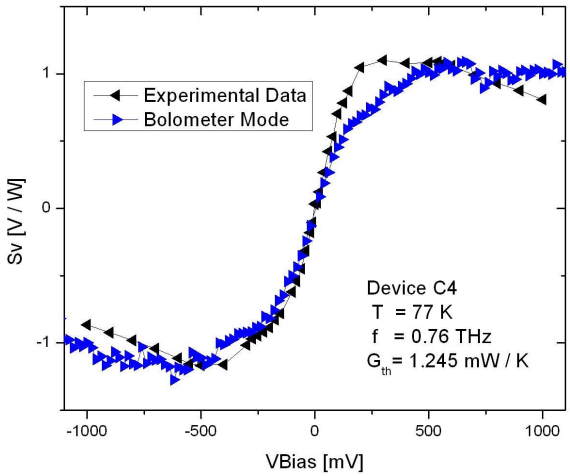

Figure 16. Plot of the measured responsivity of device C4 versus bias voltage (black points) compared with the prediction from the bolometer model (blue points). Detection was measured at 77 K at 0.76 THz.

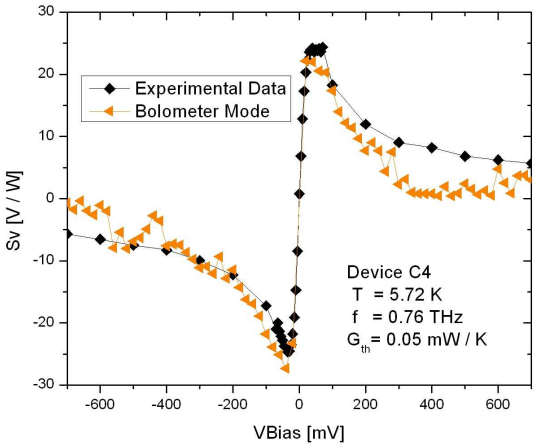

Figure 17. Plot of the measured responsivity of device C4 versus bias voltage (black points) compared with the prediction from the bolometer model (orange points). Detection was measured at 5.7 K at 0.76 THz

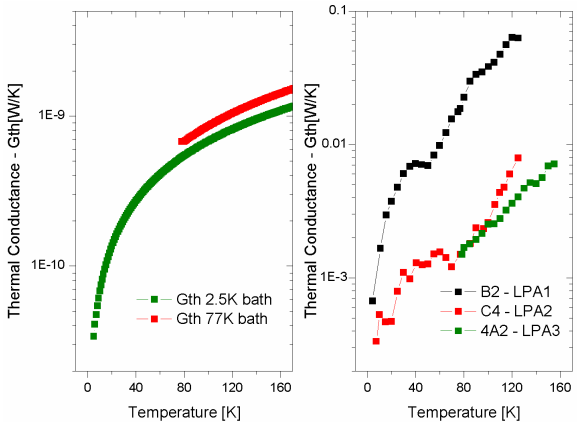

Figure 18. Plots of G_{th} measured for single SWCNTs in [5,6] (left). Plots of G_{th} versus temperature as derived from fits to Eq. (3) for three of our devices.

However, the values we obtain for G_{th} are about five to six orders-of-magnitude larger than for a single tube. To understand this we need to modify Eq. (3) to take into account additional effects that may occur.

$$S_V^{(1)} = \Delta V / P_{THz,abs} = \frac{V_0 * b}{[G_{th} + i\omega C]} \left[\frac{\eta}{L_{opt} L_{mism}} \right] (V/W) \quad (4)$$

First, the devices we measured consisted of a number of tubes which will increase the total thermal conductance. We do not presently have an accurate estimate for the effective number of tubes, but it is likely to be in the range 10-100 (see Table I). The thermal conductance of bundles of tubes, as versus single tubes, is not well known. Any optical (L_{opt}) or mismatch (L_{mism}) losses to the THz radiation would also be interpreted as an increased G_{th}, as indicated in Eq. (4). In [15] we estimated such losses to be about 16 dB. A more accurate estimate would require having better models for terahertz propagation on CNTs in bundles than we presently have. Finally, the factor η is introduced to take into account the efficiency with which electrons that are heated in the CNTs are able to diffuse out and tunnel through the contacts, a factor that is very difficult to estimate. To fully account for our data, η may have to be assumed to be quite small. One factor that may also influence the coupling loss (L_{mism}) is if terahertz energy is lost from the active metallic tubes to other inactive tubes in the bundles.

D.Devices That Conform to The Diode Model

We found two devices for which the diode models produced good fits to the measured $S_V(V_{bias})$. An example is shown in Figure 19 below (device 4A2). The fit is good except for some deviation at the highest voltages that may be due to an additional bolometric effect. However, it is clear that the bolometer model does not fit the data over-all. Similar fits were obtained for this device at 0.76 THz, 1.27 THz and 1.63 THz. Interestingly, when the same device was measured at 5.7 K, we found that both models could be used to fit the data.

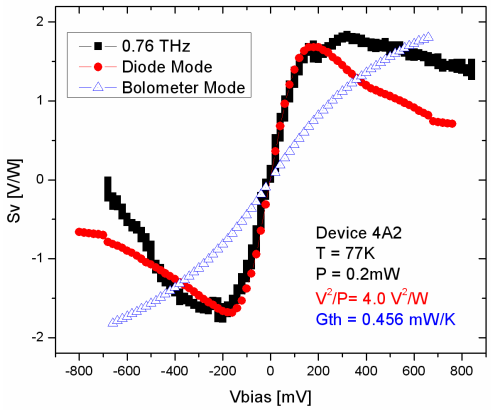

Figure 19. Measured responsivity of device 4A2 versus bias voltage (black) compared with predictions from diode model (red) and bolometer model (blue points). Detection measured at 77K and 0.76THz.

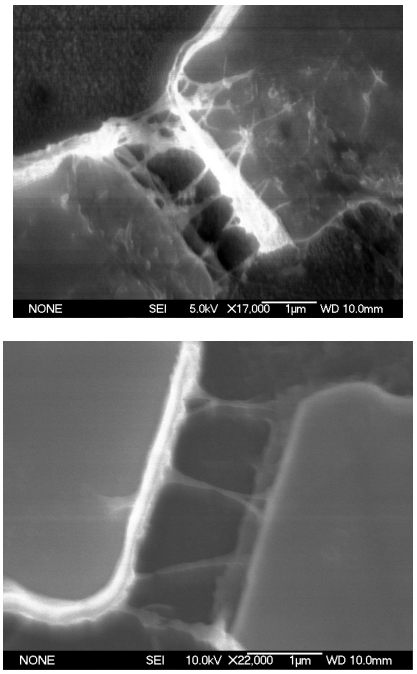

Figure 20. SEM pictures of devices that showed bolometric detection (top) and diode mode detection (bottom). Scale bar: 1µm.

This is the first time, as far as we know, that diode mode detection in CNTs has been demonstrated at such high frequencies. We ascribe this detection to the contact nonlinearities, as outlined in Sec. III.A. Figure 20 shows two

devices of which the one at the top showed bolometer mode detection, while the one at the bottom showed diode mode detection. Both devices that showed diode mode detection have tubes that appear to terminate on the edges of the antenna as the one shown in Figure 20. However, some devices that appear similar to the diode mode devices in SEM pictures also conform to the bolometer mode, so this question requires further study.

The diode model fits and the measured IV-curves enable us to obtain estimated values of the factor V^2_{THz}/P_{THz} in Eq. (2). With a given antenna impedance of 100 Ω, this factor should ideally be 200 Ω, if the entire terahertz voltage were coupled to the contacts (note that V_{THz} in Eq. (2) is the peak value). From the fits to the experimental data we instead find V^2_{THz}/P_{THz} = 8.0, 5, and 1.7 Ω at 0.76 THz, 1.27 THz, and 1.63 THz, respectively. We have corrected these values for an estimated 3 dB of optical loss in order to find the intrinsic values, at the antenna terminals. The best result (at 0.76 THz) corresponds to a 14 dB coupling loss for the THz power, significantly better than the total efficiency for the bolometer devices. To analyze the coupling loss of our diode mode devices we use a circuit model shown in Figure 21, based on the transmission line (TL) model for the high-frequency properties of SWCNTs from P. Burke [26]. The model has been modified by assuming nonlinear contact resistances, R1 and R2, with parallel contact capacitances, C1, and C2. Between the contacts we insert the Burke TL model for the m-SWCNT. This model assumes that the electron coupling effects in the m-SWCNT produce a Tomonaga-Lüttinger plasmon propagation mode for the electrons with a propagation velocity of about $2.4*10^6$ m/s. Plasmon resonances are predicted whenever the CNT length is a multiple of half the plasmon wavelength [26]. We have simulated this model using the ADS package [27]. We used contact resistances that match the measured DC resistance, R_{CNT} = 2 kΩ in agreement with [28], tube length of 1.3 µm, a plasmon velocity of $2.4*10^6$ m/s [26], and a characteristic impedance of the TL of 9.7 kΩ. We also assumed ten SWCNTs thus modelled, connected in parallel (Figure 21 for simplicity shows only one of these).

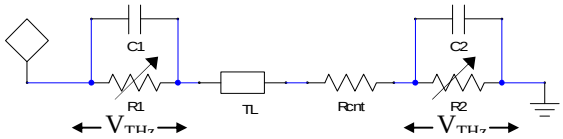

Figure 21. Circuit model for the m-SWCNT operating in the diode mode.

The main characteristic of the measured data is that the responsivity decreases as the frequency increases. If we initially neglect the effect of the plasmon transmission line, but not the m-SWCNT resistance, R_{CNT}, then this decrease could be caused by shunting of the contact resistance due to the contact capacitance. This case is illustrated in Figure 22.

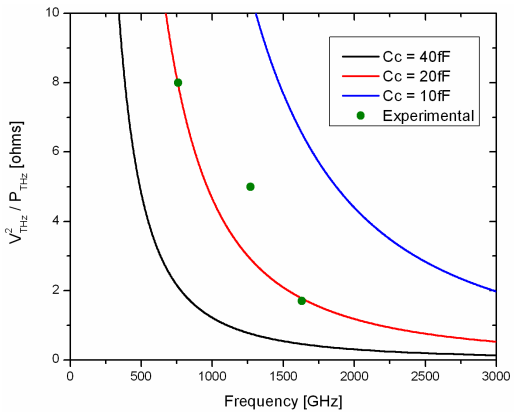

Figure 22. Simulation of the circuit in Figure 21 for the case that the plasmon TL is neglected. The green points are experimentally measured, and corrected for optical loss.

The measured data could thus be explained if the contact resistance was about 20 fF, a somewhat high value, but within the range of values we have measured at microwave frequencies [15]. Of, course, there may also be other unknown frequency-independent loss mechanisms such as particles from the original CNT solution, etc. If there were such losses, the capacitance value required would be smaller. The validity of the plasmon model has not been completely demonstrated yet, which is why we might neglect the TL. For example, McEuen et al. [12] detected resonances on a SWCNT using time-domain terahertz spectroscopy, but obtained a propagation velocity equal to the Fermi velocity, more than three times faster than the predicted plasmon velocity. This would shift the resonances to higher frequencies by that factor.

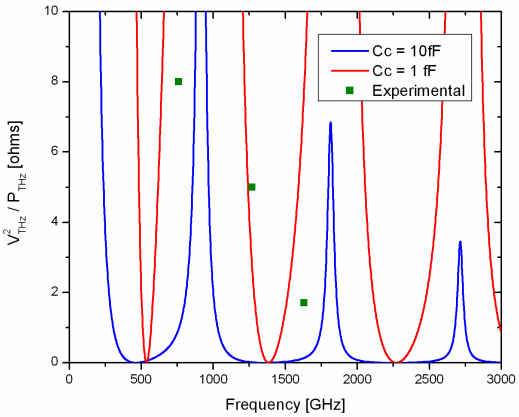

Figure 23. Simulation of the circuit in Figure 21 for the case when the plasmon TL is included. The green points are again experimentally measured.

We next compare a simulation with the plasmon TL model included, see Figure 23. In this case, the plasmon resonances clearly have a major effect on the voltage across the contacts. The experimental data are fairly close to the red curve for C_c (= C1+C2) = 1 fF. Measurements at a few more frequencies would quickly establish which of these general pictures (Figure 22 or Figure 23) is more correct. The main point here is that for devices that detect in the diode mode it should be feasible to check this type of circuit models, and answer questions such as what the propagation velocity is, does the TL model apply to bundles of tubes, etc.. We note that [29] and [30] predict yet again different values for the TL propagation velocity. In any case, it appears much more

straightforward to do this type of model fitting for the diode mode than for the bolometer mode. The circuit model fitting to terahertz data could also be combined with further microwave measurements, as we did in [15].

V. PROGRESS IN LARGE-SCALE ATOMISTIC SIMULATION

In order to obtain the different component characteristics presented in the equivalent circuit model in Fig.21, we aim to go beyond the current state-of-art capabilities for simulating CNTs by developing large-scale *ab-initio* atomistic approaches. Our proposed atomistic Density Functional Theory (DFT) and Kohn-Sham equation approach has the potential to clear up our understanding of many experimental issues, and to offer the high degree of reliability and accuracy needed to characterize the following macroscopic quantities: kinetic inductance, contact resistance and contact capacitance, quantum capacitance and CNT resistance.

An atomistic description of a long CNT up to 100nm (~ 10,000 atoms), which has been so far considered as a formidable task, could however provide important insights into the electronic properties of the device. In order to achieve this goal efficiently, we have been developing innovative numerical modeling strategies using a real-space mesh technique framework and a combination of mathematical methodologies and high-performance parallel algorithms such as the CMB strategy [31,32] (CMB stands for mode approach/contour integration/banded solver). Using our CMB strategy, the typical electron density of 20nm long CNT composed by ~2500 atoms can be computed in only`90 seconds using only one core of current workstation which is orders of magnitude faster than any other existing *ab-initio* techniques. In addition the CMB strategy is fundamentally designed for making a competitive parallel implementation possible at different levels of the modeling process.

Recently, a highly efficient and innovative numerical algorithm for solving the symmetric eigenvalue problem, FEAST, has been proposed and described in detail in [33]. This general algorithm is fundamentally different from the traditional Krylov subspace iteration based techniques and takes its inspiration from the density matrix representation and the contour integration techniques in quantum mechanics. In contrast to the CMB strategy, FEAST can calculate all the eigenpairs (eigenvalues and eigenvectors) and its main computational tasks consist of solving few (standard) independent linear systems with multiple right-hand sides along the complex contour. Using the mode approach, the obtained banded linear systems can be solved using highly efficient SPIKE-based algorithm [34]. .TABLE II summarizes the timings obtained for computing the electron density of a (5,5) CNT using both the CMB strategy and the FEAST algorithm. Both algorithms exhibit linear scaling performances when the size of the system increases and can then be potentially used to simulate very long CNTs. CMB is faster than FEAST but this latter is more accurate since it provides as well all the exact eigenpairs (i.e. the integration along the complex contour benefits from an iterative refinement technique which minimizes the numerical quadrature error).

#unit cells	1	3	6	24	48
N	199,874	331,298	528,434	1,711,250	3,288,338
$N_1 * M$	6278	9438	14861	48125	92477
$L(nm)$	0.73	1.23	1.98	6.51	12.55
$\#atoms$	20	60	120	480	960
T_{CMB} (s)	2.24	3.26	4.87	16.5	30.1
T_{FEAST} (s)	10.2	15.0	24.6	221	491

TABLE II. Comparisons of the simulation times for computing the electron density of a metallic (5,5) CNT using the CMB strategy and the FEAST algorithm which computes all the eigenpairs. The calculations are performed using only one core of an Intel-Clovertown system (2.66GHz, 16Gb).

In order to illustrate the efficiency of our modeling technique for handling both finite and periodic systems, we have compared in Figure 24 the density of states (DOS) of the (5,5) CNT calculated using (i) the bandstructure diagram of periodic (infinite) system, (ii) the histogram of all the eigenvalues obtained considering different lengths for the tube as reported in TABLE II. . As expected, the numerical results between the periodic and finite systems become closer as the length of the CNT increases. The boundary effects at the edge of the finite tube are noticeable for short-lengths where they let appear some states in the region around the Fermi-level which is in principle flat (constant) for the periodic system. These effects/states almost completely disappear for the 48-unit cell CNT.

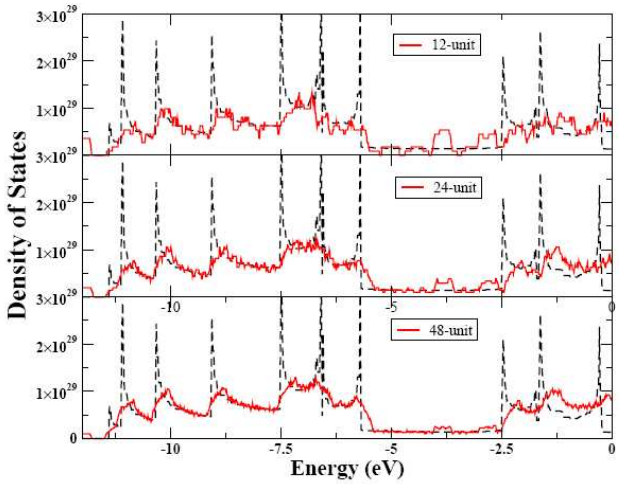

Figure 24. Comparisons of the density of states obtained for the periodic (5,5) CNT and the finite (5,5) CNT (isolated system) using three different length 12-unit, 24-unit and 48-unit cells

In order to perform the time-dependent simulations using TDDFT calculations (Time dependent DFT), we have recently investigated two different numerical strategies: (i) a scheme based on the Crank Nicolson procedure that will allow us to adapt the transient simulation approach proposed in [35], and (ii) a scheme based on spectral decomposition (solving the integral equation). This latter associated with innovative numerical quadrature techniques for decomposing the time evolution operator, shows promises for simulating long time-scale and then capturing the essential physics of the terahertz experimental data [36].

VI. Conclusion

We have demonstrated detection of terahertz radiation in a number of devices that couple integrated antennas to CNTs. The DEP fabrication is very convenient and reliable. While the voltage responsivity, which is interpreted as due to a bolometer effect, is much lower than for similar microwave devices [3],[4], the present configuration enables a variety of studies of CNTs at THz frequencies. The new demonstration of diode mode detection up to 1.6 THz shows stronger coupling of the terahertz radiation to the CNTs and should be useful for exploring the high-frequency models of m-SWCNTs, such as the properties of the Tomonaga-Lüttinger liquid plasmons, in future work. We are presently working on fabrication methods that should result in low-resistance contacts to both bundles and single tubes, and much higher responsivities are expected, as discussed in Sections II and III. These experimental studies will be interpreted with the help of the *ab initio* simulations. A final step is the expansion to heterodyne detectors and the first determination of the thermal time-constant of m-SWCNT detectors (in the frequency domain). The time-constants are expected to be very short [1,2].

References

[1] K.S. Yngvesson, "A New Hot Electron Bolometer Heterodyne Detector Based on Single-Walled Carbon Nanotubes," *16th Intern. Symp. Space Terahertz Technol.*, Göteborg, Sweden, May 2005, p. 531.

[2] K.S. Yngvesson, "Very wide bandwidth hot electron bolometer heterodyne detectors based on single-walled carbon nanotubes," *Applied Phys. Lett*, vol. **87**, p. 043503 (2005).

[3] K.S. Yngvesson, F. Rodriguez-Morales, R. Zannoni, J. Nicholson, M. Fishetti, and J. Appenzeller, "Microwave Detection and Mixing in Metallic Single Wall Carbon Nanotubes and Potential for a New Terahertz Detector," *17th Intern. Symp. Space Terahertz Technol.*, Paris, France, May 2006, p. 135.

[4] F. Rodriguez-Morales, R. Zannoni, J. Nicholson, M. Fischetti, K. S. Yngvesson, and J. Appenzeller, *Appl. Phys. Lett*. **89**, 083502 _2006_.

[5] D.F. Santavicca and D. Prober, "Terahertz Resonances and Bolometric Response of a Single Walled Carbon Nanotube", paper 1646, 33rd Intern. Conf. Infrared, Millimeter and Terahertz Waves, Sept. 2008, CalTech, Pasadena, CA.

[6] D.F. Santavicca, J. Chudow, A. Annunciata, L. Frunzio, D. Prober, M. Purewal and P. Kim, "Terahertz resonances on a single-walled carbon nanotube," Intern. Workshop on Optical Terahertz Science and Technol., Santa Barbara, CA, March 7-11, 2009.

[7] H.M. Manohara, E.W. Wong, E. Schlecht, B.D. Hunt, and P.H. Siegel, *Nano Lett.* **5**, 1469 (2005).

[8] S. Rosenblatt, H. Lin, V. Sazonova, S. Tiwari, and P.L. McEuen, *Appl. Phys. Lett*. **87**, 153111 (2005).

[9] A. A. Pesetski, J.E. Baumgardner, E. Folk, J. Przybysz, J. D. Adam, and H. Zhang, *Appl. Phys. Lett.*, **88**, 113103 (2006).

[10] M. Tarasov, J. Svensson, L. Kuzmin, and E. E. B. Campbell, *Appl.Phys.Lett.*, **90**, 163503 (2007).

[11] C. Rutherglen and P. Burke, "Carbon Nanotube Radio," *Nano Letters*, **7**, p. 3296 (2007).

[12] Z. Zhong, N.M. Gabor, J.E. Sharping, A.L. Gaeta, and P.L. McEuen, "Terahertz time-domain measurement of ballistic electron resonance in a single-walled carbon nanotube," *Nature Nanotechnol.* **3**, 201 (2008).

[13] M.E. Itkis, F. Borondics, A. Yu and R.C. Haddon, *Science*, **312**, 413 (2006).

[14] K. Fu, R. Zannoni, C. Chan, S.H.Adams, J. Nicholson, E. Polizzi and K.S. Yngvesson, "Terahertz detection in single wall carbon nanotubes," *Appl. Phys. Lett.*, **92**, 033105 (2008).

[15] K.S. Yngvesson, K. Fu, B. Fu, R. Zannoni, J. Nicholson, S.H. Adams, A. Ouarraoui, J. Donovan and E. Polizzi, "Experimental detection of terahertz radiation in bundles of single walled carbon nanotubes," Proc. 19th Intern. Symp. Space Terahertz Technol., Groningen, The Netherlands, April 28-30, 2008, p. 304.

[16] K. Fu, "Metallic Carbon Nanotubes, Microwave Characterization and Development of a Terahertz Detector," *M.Sc. thesis, University of Massachusetts, Amherst, MA* (2008).

[17] Z. Yao, C.L. Kane, and C. Dekker, *Phys. Rev. Lett.* **84**, 2941 (2000).

[18] Th. Hunger, B. Lengeler, and J. Appenzeller, Phys. Rev. B, **69**, 195406 (2004).

[19] E. Pop, D.A. Mann, K. Goodson, and H. Dai, J. Appl. Phys., **101**, 093710 (2007).

[20] R. Krupke and F. Hennrich, *Adv. Eng. Mater*. **7**, 111 _2005.

[21] E. Gerecht, C. Musante, Y. Zhuang, K. Yngvesson, T. Goyette, J. Dickinson, J. Waldman, P. Yagoubov, G. Gol'tsman, B. Voronov, and E. Gershenzon, *IEEE Trans. Microwave Theory Techn.*, vol. **47**, pp. 2519–2527, (1999).

[22] Cheap Tubes, Brattleboro, Vt.. Purified 90% SWCNTs, grown by CVD, nominal diameter from 1 to 2 nm., average length of 50 μm before ultrasonication.

[23] K.S. Yngvesson, "*Microwave Semiconductor Devices*", Kluwer Academic, Norwell, MA (1991).

[24] P.L. Richards, *J. Appl. Phys*., **76**, 1 (1994).

[25] S. Yngvesson and E. Kollberg, "Optimum Receiver Noise Temperature for NbN HEB Mixers According to the Standard Model," *10th International Symposium on Space THz Technology*, Charlottesville, VA, March 1999, pp. 566-582.

[26] P. J. Burke, "Lüttinger liquid theory as a model of the gigahertz electrical properties of carbon nanotubes," *IEEE Trans. Nanotech*. **1**, 129 (2002).

[27] Agilent, Inc., Santa Clara, CA.

[28] M. S. Purewal, B. H. Hong, A. Ravi, B. Chandra, J. Hone, and P. Kim, "Scaling of Resistance and Electron Mean Free Path of Single-Walled Carbon Nanotubes", *Phys.Rev.Lett*. **98**, 186808 (2007).

[29] G.W. Hanson, "Fundamental Transmitting Properties of Carbon Nanotube Antennas", *IEEE Trans. Antennas Propagat.*, **53,** 2426 (2005).

[30] M. V. Shuba, S. A. Maksimenko and A. Lakhtakia "Electromagnetic wave propagation in an almost circular bundle of closely packed metallic carbon nanotubes" *Phys. Rev. B*., **76,** 155407 (2007).

[31] D. Zhang and E. Polizzi, "Efficient Modeling Techniques for Atomistic-Based Electronic Density Calculations", J. Comp. Elec., Vol. 7, N. 3, pp 427-431 (2008).

[32] D. Zhang and E. Polizzi, "Linear scaling techniques for first-principle calculations of large nanowire devices", 2008 NSTI Nanotechnology Conference and Trade Show. Technical Proceedings, Vol. 1 pp12-15 (2008).

[33] E. Polizzi, "Density-Matrix-Based Algorithms for Solving Eingenvalue Problems" Phys. Rev. B. Vol. 79, 11512 (2009).

[34] E. Polizzi, A. Sameh. "A Parallel Hybrid Banded System Solver: The SPIKE Algorithm", *Parallel Computing*, **32**, 2, pp. 177-194 (2006).

[35] O. Pinaud, "Transcient simulations of resonant tunneling diode", *J. Appl. Phys.* **92**,1 p1987 (2002).

[36] Z. Chen, E. Polizzi, (unpublished,).